

Model Predictions for Clustering and Morphologies at HDF depths

By MATTHIAS STEINMETZ

Steward Observatory, University of Arizona, Tucson, AZ 85721, USA

The current status of numerical simulations of the formation of galaxies is reviewed. Success and failure of modeling galaxies at low and high redshift is demonstrated using a variety of examples, such as the Tully-Fisher relation, the appearance of high-redshift galaxies and the kinematics of damped Ly α systems. The relationship between the clustering properties of high- z galaxies and the present generation of galaxies is emphasized.

1. Introduction

Hierarchical clustering is at present the most successful paradigm of structure formation in the universe. In this scenario – Cold Dark Matter (CDM) and its variants are perhaps the best known examples – structure grows as systems of progressively larger mass merge and collapse to form newly virialized systems. A large variety of models which are based on the hierarchical clustering hypothesis have been extensively studied using N-body simulations as well as analytical approximations.

Within the last few years, more and more work focussed on smaller structures, and tried to embed galaxy formation into the hierarchical picture. One successful approach has been semi-analytical or phenomenological models (Kauffmann, White & Guiderdoni, 1993; Cole et al., 1994). These models use the extended Press-Schechter theory to predict abundances and merger rates of halos as a function of mass and redshift. Physically motivated recipes are used to model how gas cools, how it settles at the center of dark matter halos and how it is transformed into stars. This phenomenological ansatz provides at comparably low computational cost a very efficient method to predict the formation and evolution of the galaxy population. However, it has only little power in predicting the clustering of galaxies (see, however, Kauffmann, Nusser & Steinmetz, 1997) and it makes no prediction on the detailed formation history of individual galaxies.

Detailed studies of the formation of individual galaxies necessarily require large numerical simulations which include not only gas dynamics, shocks and radiative cooling, but which also incorporate some description of star formation. This article addresses some successes and failures of such simulations. It will focus on issues which seem to be generic to the hypothesis of hierarchical clustering and which depend only little on the details on the underlying cosmogony. Numerical details are discussed in the appendix.

2. Prologue: The Overcooling Problem

Already the very first quantitative investigations of galaxy formation in hierarchically clustering universes (e.g., White & Rees 1978) exhibited a generic problem of this class of models, nowadays usually referred to as the *overcooling problem*. Since cooling times scale inversely with density, the dissipative collapse of gas must have been more efficient at high redshift because the dark matter halos present at that time (and the universe as a whole) were denser. Cooling is expected to be so efficient at early times that almost all gas within a dark matter halo is able to cool to temperatures of about 10^4 K. Consequently, galaxies tend to be too massive. A related problem is that hierarchical models predict

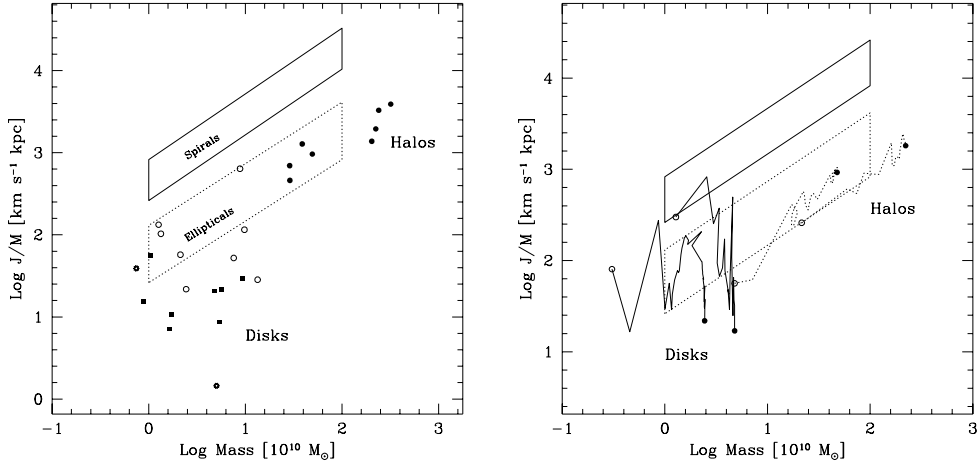


FIGURE 1. Left: The specific angular momentum of dark halos and gaseous disks, as a function of mass. The boxes enclose the region occupied by spiral and elliptical galaxies, as given by Fall (1983). Open circles correspond to runs without UV background; solid squares correspond to a soft UV background ($J_{-21} = 1$, $\alpha = 5$ (equation 2.3)), starred symbols correspond to an extremely energetic background ($J_{-21} = 10$, $\alpha = 1$). Note that the halos' J/M scale approximately as $M^{2/3}$, as expected if all systems had the same value of the rotation parameter λ (see text for a definition). Gaseous disks have much lower angular momenta than observed spirals, a consequence of the role of mergers during the assembly of the disks. Note that the inclusion of a UV radiation field seems to aggravate this problem. Right: Evolution of the dark halo and central gaseous disk in the J/M versus M plane, from $z = 5$ (open circles) to $z = 0$ (solid circles). The mass of the system grows steadily by mergers, which are accompanied by an increase in the spin of the halo and a decrease in the spin of the central disk. The latter results from angular momentum being transferred from the gas to the halo during mergers.

an overabundance of low mass halos with circular velocities below 100 km/s (Cole et al., 1994).

This can be quantified by the following analytical argument (see, e.g., White 1994). At a given redshift z , the mass of a dark matter halo of circular velocity v_c can be written as

$$M_{\text{vir}} = 2.6 \times 10^{12} M_{\odot} \frac{3\zeta}{2} h^{-1} (1+z)^{-1.5} \left(\frac{v_c}{220 \text{ km/s}} \right)^3, \quad (2.1)$$

the factor ζ representing the age of the universe in units of H_0^{-1} , i.e., for a $\Omega = 1$ universe $\zeta = 2/3$. Following White et al. (1993), the baryon fraction ($M_{\text{bary}}/M_{\text{tot}}$) within the virial radius should be very similar to the cosmological value Ω_b/Ω_0 , with the nucleosynthesis value $\Omega_b = 0.0125 h^{-2}$. The baryonic mass enclosed in a halo of circular velocity v_c is thus given by

$$M_{\text{bary}} = \frac{\Omega_{\text{bary}}}{\Omega_0} M_{\text{vir}} = 3.3 \times 10^{10} M_{\odot} \frac{3\zeta}{2\Omega_0} h^{-3} (1+z)^{-1.5} \left(\frac{v_{\text{vir}}}{220 \text{ km/s}} \right)^3. \quad (2.2)$$

Let us apply this to the case of the Galaxy. By assuming that the circular velocity of the dark matter halo is similar to the actual rotation velocity of the Galactic disk ($M_{\text{disk}} \approx 6 \times 10^{10} M_{\odot}$), the following statements can be made:

- In the case of $\Omega_0 = 1$ and $h = 0.5$, the total baryonic mass amounts $2.6 \times 10^{11} M_{\odot}$,

i.e., 4 times the mass of the galactic disk. For $\Omega = 0.2$, $\Lambda = 0.8$ the situation is even more extreme, the total baryonic mass is $2.1 \cdot 10^{12} M_{\odot}$, i.e., only 3% of the baryonic mass has cooled and settled into the disk.

- The situation is a bit less extreme if a higher h and/or a lower Ω_b is assumed, as, e.g., favored by recent Deuterium measurements by Songaila et al. (1994). Vice versa, even less gas has cooled if a higher Ω_b is assumed, as, e.g., favored by the Deuterium measurements of Tytler, Fan & Burles (1996).

- Since the cooling radius of a Milky Way sized system includes much more mass than the mass of the disk, a very efficient heating mechanism has to be postulated to prevent a large fraction of the baryonic mass from cooling.

- It is of some interest to note that for $\Omega = 1$ and $h = 0.8$ there exist hardly enough baryons to account for the mass observed in the galactic disk.

This simple model nicely reproduces the main feature seen in numerical simulation of galaxy formation (see, e.g., Navarro & Steinmetz 1997), namely that virtually all baryons within a dark matter halo are able to cool resulting in disk galaxies which are too massive.

Numerical simulations also show another shortcoming of the hierarchical clustering hypothesis, which is to some extent related to the overcooling problem: the angular momentum of simulated galaxies is too small. Compared to their observed counterparts galaxies are thus too concentrated. This is shown in figure 1 which shows the specific angular momentum of dark matter halos and of their central gaseous disks at $z = 0$, as a function of mass. The boxes indicate the loci corresponding to spiral and elliptical galaxies, as compiled by Fall (1983). If, as suggested by Fall & Efstathiou (1980), the collapse of gas would proceed under conservation of angular momentum, the baryonic component would have the same specific angular momentum J/M as the dark matter, however, its corresponding mass would be a factor of 20 smaller (for $\Omega_{\text{bary}} = 0.05$, $\Omega_0 = 1$). These disks would be located only slightly below the box for spiral galaxies. However, figure 1 demonstrates clearly that the spins of gaseous disks are about an order of magnitude lower than that. This is a direct consequence of the formation process of the disks (Navarro, Frenk & White 1995). Most of the disk mass is assembled through mergers between systems whose own gas component had previously collapsed to form centrally concentrated disks. During these mergers, and because of the spatial segregation between gas and dark matter, the gas component transfers most of their orbital angular momentum to the surrounding halos (Frenk et al., 1985; Barnes 1988; Quinn & Zurek 1988).

As already mentioned, efficient feedback processes are required to prevent the gas from excessive cooling. One proposal has been that energy input due to a photoionizing UV background may prevent cooling in low mass halos at higher redshift (Efstathiou 1992). This hypothesis has been tested by numerical simulations but came to a negative result (Quinn, Katz & Efstathiou 1996; Weinberg, Hernquist & Katz 1997; Navarro & Steinmetz 1997). These simulations assumed the presence of a photoionizing background with an energy distribution

$$J(\nu) = J_{-21} \times 10^{-21} \left(\frac{\nu}{\nu_H} \right)^{-\alpha}. \quad (2.3)$$

Though an UV background can delay or even prevent the formation of galaxies with circular velocities of 30-50 km/s and below, its influence on the properties of galaxies with circular velocities exceeding 100 km/s is almost negligible. The amount of cool gas is only moderately reduced by about 10-30%. For extreme assumptions on the UV background it can be reduced by 50%, insufficient to reconcile the observed shape of

the galaxy luminosity function. Concerning the angular momentum of gaseous disks, a UV background even exacerbates the angular momentum problem as shown by the solid squares and starred symbols in figure 1. This can be easily understood, since gas which falls in late and thus has low densities is most strongly affected by the UV background. Such gas, however, also possesses the highest specific angular momentum.

To solve the overcooling/angular momentum problem thus energy feedback from supernovae has been repeatedly advocated (e.g., Dekel & Silk 1986). The stumbling block for implementing star formation into galaxy formation simulations is certainly the ill-understood physics of star formation and the interaction of evolving stars with the ISM. The negative effect of photoheating on the angular momentum of cold disk also points to an interesting complication which seem to be generic to quite a variety of feedback mechanisms: In order to explain the observed sizes of disk galaxies, the specific angular momentum of the disk must not be much smaller than that of the host dark matter halo. However, it is also gas at large radii which (i) possesses the highest specific angular momentum and which (ii) has the lowest density and for which cooling can be easily suppressed. It is thus a non-trivial problem how the amount of cool gas can be reduced by a large fraction without affecting its specific angular momentum. This problem seems to be especially severe for low- Ω_0 models, where only a small fraction of baryons can be allowed to cool. In the following sections, some results from simulations including star formation and feedback are being discussed. These simulations incorporate supernova feedback due only to thermal energy (see appendix). To some extent they can thus be considered as minimum feedback models.

3. Simulation Sample

The galaxy sample which is analyzed in the following sections consists of 21 galaxies with circular velocities between 50 and 250 km/s. This sample has been compiled from a set of 8 high resolution numerical simulations. The mass of a gas particle is between $5 \times 10^6 M_\odot$ and $2 \times 10^7 M_\odot$, the gravitational softening is 1 kpc. The star formation efficiency has been calibrated so that at $z = 0$ a galaxy with a circular velocity of 200 km/s has a star formation rate of about $1 M_\odot/\text{yr}$. Details of the numerical method and the star formation and feedback scheme are presented in the appendix. Each galaxy consists of $10^2 - 10^4$ star particles. Each of these particles represents a population of a few million stars which have been formed in a burst-like manner, i.e., a model galaxy can be considered as a superposition of several thousand mini starbursts. Each star particle is labeled by an age (time since creation) and a metallicity equal to that of its gas progenitor at the time of formation. The luminosity evolution of each of these bursts is then followed by an evolutionary spectral synthesis model (Contardo, Steinmetz & Fritze-von Alvensleben 1998). The model galaxies can thus be “observed” in arbitrary colors. The power of this technique is illustrated in Figure 2, which shows a computer-generated rendition of a CDM-dominated universe observed with the Hubble Space Telescope (HST) with exposures similar to those used for the Hubble Deep Field (HDF). The image contains galaxies of various intrinsic luminosities, placed at different redshifts and taken from the simulation sample so as to reproduce approximately the apparent magnitude and redshift distributions of galaxies in the HDF. The image includes realistic noise levels, and has been processed with a point-spread function (PSF) similar to that of HST. This image illustrates dramatically how simulations can be “observed” and compared directly with high-resolution observations of distant galaxies.

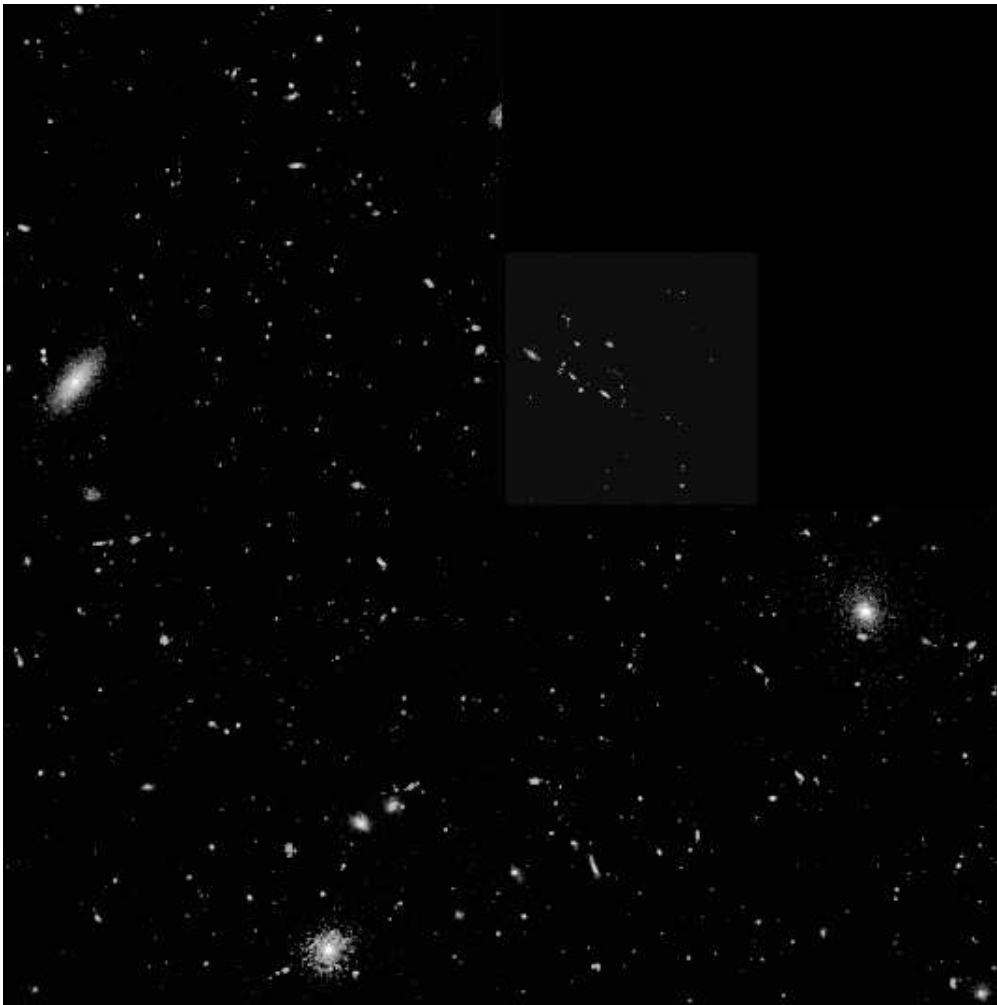


FIGURE 2. Computer-generated synthetic image of a WFPC2/PC field with parameters chosen to match the exposures corresponding to the Hubble Deep Field (HDF). All bands observed in the HDF have been simulated and combined to produce this image. The cosmological model probed is standard CDM.

4. Tully-Fisher Relation

The Tully-Fisher (TF) relation in several colors provides an excellent testbed for galaxy formation simulations. The total baryonic mass of a dark-matter halo scales with its circular velocity like $M \propto v^3$ (equation 2.2), and thus already provides a scaling similar to the observed luminosity/velocity relation (see, however, Silk (1997) for a model in which the TF relation arises mainly as a consequence of self-regulated star formation in galactic disks). This basic relation is then modulated by the mass distribution of the gas compared to the dark matter (i.e., the relation between the actual rotation velocity of gas/stars and the virial velocity of the dark-matter halo), the efficiency of transforming gas into stars and the mass-to-light ratios in different bands. All these modulations are likely to depend on the mass (or, equivalently, circular velocity) of the halo and will affect the normalization, scatter, and slope of the TF relation. Hence, the kinematic of galaxies

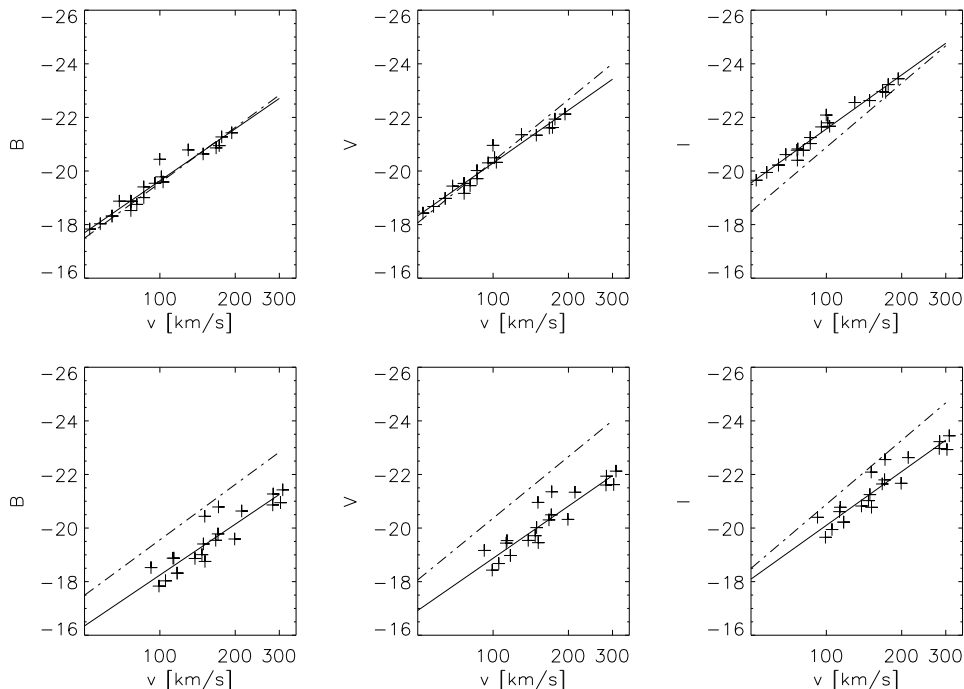


FIGURE 3. Tully-Fisher relation: B (left), V (middle) and I (right) luminosity of numerically simulated galaxies versus their circular velocity at the virial radius (top row) and their maximum rotation velocity (bottom row). The solid lines correspond to a least square fit to the simulated data, the dash-dotted lines correspond to the observed B,V and I Tully-Fisher relation (from Pearce & Tully, 1992).

(represented by their rotation velocities) is linked with their current star formation rate (represented by their B-band luminosities), and their star formation history (represented by their I or K-band luminosities). Finally, these modulations have to preserve the small scatter of about 0.3 mag in the observed TF relation. Further constraints can be derived by comparing the redshift evolution of the TF relation with observations (e.g., Vogt et al., 1997).

Figure 3 shows the B-, V- and I-band TF relation for the numerically simulated galaxies. In order to demonstrate different contributions, the B, V and I luminosities are plotted against the circular velocity of the DM halo and against the maximum velocity of the rotation curve. For comparison a best fit to the simulated data (solid line) and the observed data (dashed line, from Pierce & Tully 1992) is shown. The plot demonstrates that the simulations can qualitatively reproduce many features of the observed data: first of all, a clear steepening of the TF relation from B to I is visible. While the luminosity is proportional to $L_B \propto v^{2.4}$, the I luminosity follows $L_I \propto v^{2.7}$. Also the *rms* scatter is remarkably small, 0.2 mag, if using the virial velocity and 0.4 mag using the maximum rotation velocity. These data are consistent with the observed values of $\Delta M = 0.3$ mag (recall, dark matter halos obey $\Delta M = 0$ mag and $M \propto v^3$). Slope and scatter of the TF relations as well as differences between different bands are a result of the simulations. The calibration of the star formation law only enters by fixing the B luminosity of a galaxy within a halo of circular velocity 200 km/s !

However, a more quantitative comparison shows that the model fails in detail. First of all, the slope of the TF relation is too flat, especially in the I band ($L_I \propto v^{2.7}$ versus observed $L_I \propto v^{3.2}$) which probably indicates that the supernovae feedback is not acting efficiently enough. A more efficient feedback mechanism would deplete the total amount of stars at low circular velocities and thus result in a lower I-band luminosities and a steepening of the I-band TF relation. The systematically low luminosities in the lower row of figure 3 can be interpreted in two ways: either the luminosities are in fair agreement, but the galaxies are too concentrated (i.e., the maximum of the rotation curve is too high), or the velocities are in fair agreement, but the luminosities are too low. The angular momentum problem mentioned in the prologue supports the first interpretation, and also strengthens the conclusion that feedback has not worked efficiently enough. If, however, the actual rotation velocities of galaxy disks are more similar to the virial velocities of its dark matter halo, the I band TF relation (figure 3, upper right) indicates, that the total amount of stars in a galaxy of given rotation velocity is too large.

These results can be summarized as follows: the adopted feedback mechanism is too weak to resolve the overcooling/angular momentum problem. The resulting galaxies are too massive and too concentrated compared to their observed counterparts. This effect is especially strong at the low mass end and the slope of the I-band TF relation is too shallow. This discussion, however, also demonstrates how global scaling relations like the TF relation can be used to calibrate models of (large-scale) star formation and feedback in galaxy formation simulations.

5. High Redshift Galaxies

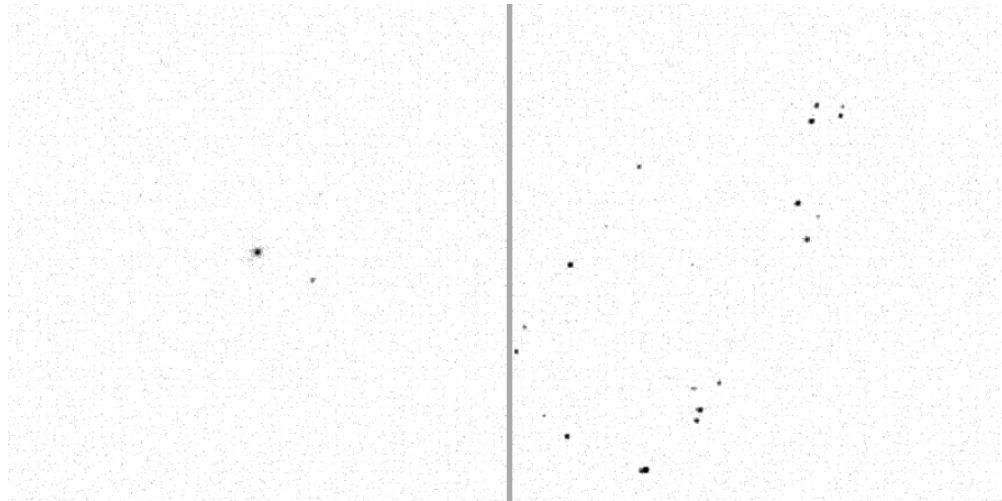


FIGURE 4. Left: Artificial I-band image of a galaxy at redshift $z=0$ as seen from a distance corresponding to $z = 3$. Right: Progenitors of this galaxies at redshift $z = 3$. The group at the lower left edge will merge to one galaxy outside the field covered by the left panel. The group near the center merges and forms the two galaxies which can be seen in the left panel. Resolution, Noise, PSF and efficiency are taken to match that of the HST WFPC2 camera, exposure time: 123.6 ksec. Each frame has a sidelength of 2.8 Mpc (comoving), corresponding to the area covered by 4 WFPC2 chips.

Although the models still fail to reproduce quantitatively the scaling relations of

present day galaxies, the qualitative agreement is probably good enough to take a closer look at the redshift evolution of these galaxies, especially if one concentrates on the high mass end where the influence of feedback processes is weaker.

Figure 4 shows a $z = 0$ galaxy and its progenitor at $z = 3$, a group of protogalactic clumps (PGCs, see also Haehnelt, Steinmetz & Rauch 1996). The baryonic masses of these clumps are only a few times $10^9 M_{\odot}$ or even less. Their mutual separation is about a few hundred kpc. All PGCs share virtually the same redshift ($\Delta v \approx 400$ km/s). Similar to the galaxy shown in figure 4, most of the 21 simulated galaxies give rise to a few detectable ($I < 26$) progenitors at $z \approx 2 - 3$, a behavior which nicely accounts for the increasing evidence for redshift clustering at redshifts above two (Pascarella et al., 1996; Steidel et al., 1997; Elston & Bechtold, 1998).

The redshift evolution of a subset of galaxies (3 galaxies with $v_c \approx 200$ km/s and 3 galaxies with $v_c \approx 80$ km/s) is shown in figure 5. By following the merging history of a galaxy, the expression "progenitor" is, of course, no longer uniquely determined for redshifts higher than that of last major merging event. Hence, at each branch in the merging tree, the more massive clump is defined as the progenitor. Luminosity, velocity and star formation rate shown in figure 5 always refers to only one bound clump.

The absolute U magnitude (figure 5, upper left) brightens with redshift about 1-2 magnitudes between redshift 0 and 2 which indicates a higher star formation rate at higher z . This assumption is confirmed by the lower left plot of figure 5 which shows the star formation rate of these clumps. At $z = 0$, the star formation rate is a very few M_{\odot}/yr for 200 km/s galaxies and an order of magnitude lower for 100 km/s galaxies. The star formation rate increases with redshift, however it always stays below a few tens of M_{\odot}/yr . Note, however, that the simulations do not account for the effects of dust.

At redshift above 2.5 a strong drop in U is visible. This dropout is mainly due to intervening absorption due to neutral hydrogen shortward of 1217 Å (restframe) and, to a smaller extent, absorption within the atmospheres of young massive stars. In R and I, the luminosity is fairly constant. The plots also indicate, that the luminosities of the more massive models are in good agreement with that of high redshift galaxies observed by Windhorst et al. (1994) and Steidel et al. (1996). Also the circular velocity of these clumps is fairly constant. The circular velocity of low v_c objects is even slightly higher at larger redshifts. Also the circular velocity of the 200 km/s galaxies increases slightly with redshift for $z < 1.5$, and it is still above 150 km/s at $z = 3$. So it should not be surprising that galaxies with velocities of a few hundred km/s exist at these redshifts (see also Steinmetz 1997; Baugh et al. 1997).

In summary, the $z \lesssim 3 - 4$ progenitors of present day galaxies have luminosities and rotation velocities similar to those of their present day counterpart. However, they are much more compact and much less massive.

6. Absorption Systems

One very successful application of gasdynamical simulations in cosmology has been the study of the intergalactic medium (IGM), in particular the physical origin of QSO absorption systems. Hydrodynamical simulations similar to those presented here explain the basic properties of QSO absorbers covering many orders of magnitude in HI column density (see, e.g., Cen et al., 1994; Katz et al., 1996; Zhang et al., 1995; Rauch, Haehnelt & Steinmetz 1997). This is also shown in figure 6 (left). While the lowest column density systems ($\log N(\text{HI}) \approx 12 - 14$, light gray) arises from gas in voids and sheets of the "cosmic web", systems of higher column density are produced by filaments ($\log N \approx 14 - 17$, dark gray) or even gas which has cooled and collapsed in virialized halos ($\log N > 17$, black).

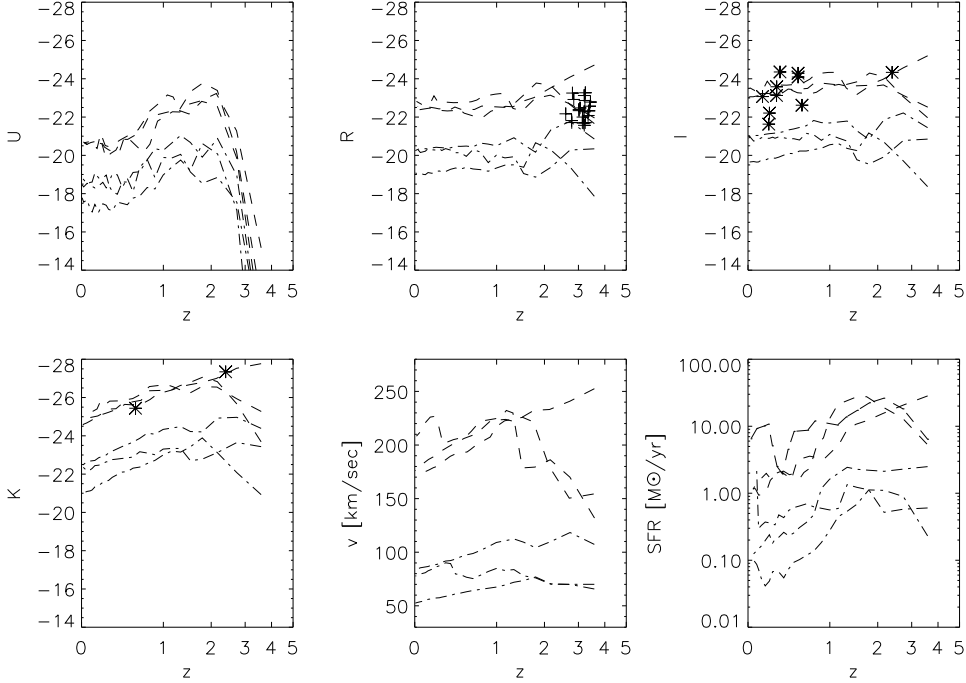


FIGURE 5. Upper row: redshift evolution of the absolute magnitude in U (left) R (middle) and I (right) of three galaxies with $v_c(z = 0) \approx 190$ km/s (dashed) and three galaxies with $v_c(z = 0) \approx 80$ km/s (dashed dotted). For comparison, (+) and (*) denoted observational data from Steidel et al. (1996) and Windhorst et al. (1994), respectively. Lower row: redshift evolution in K (left), circular velocity as a function of redshift (middle) and star formation rate as a function of redshift (right).

So far, numerical simulations have been applied primarily to systems with lower column densities ($\log N \lesssim 17$), corresponding to gas densities below 10^{-2} cm^{-3} . At such low densities the important physical processes are relatively simple and well understood. Fluctuations are still only mildly non-linear and the gas is essentially in photoionization equilibrium with the UV background. Cooling times are long compared to dynamical time scales.

The right panel of figure 6 shows the corresponding I-band image of the stellar component. The I band image includes noise, PSF and exposure time similar to that of the Hubble Deep Field. The artificial image shows about 8 detectable PGCs. Each of these PGCs is situated close to a region of very high column density ($\log N > 17$). However, there is still a substantial number of Ly-limit and damped Ly α systems, which do not host a stellar PGC.

There has been considerable debate about the physical structures giving rise to damped Ly α absorption systems (DLAS) at high redshift. DLASs have often been interpreted as large, high-redshift progenitors of present-day spirals which have evolved little apart from forming stars (Wolfe 1988). More recently, Prochaska & Wolfe (1997) have argued that only models in which the lines-of-sight (LOS) intersects rapidly rotating thick galactic disks can explain both the large velocity spreads (up to 200 km/s) and the characteristic asymmetries of the observed low ionization species (e.g., SiII) absorption profiles. In par-

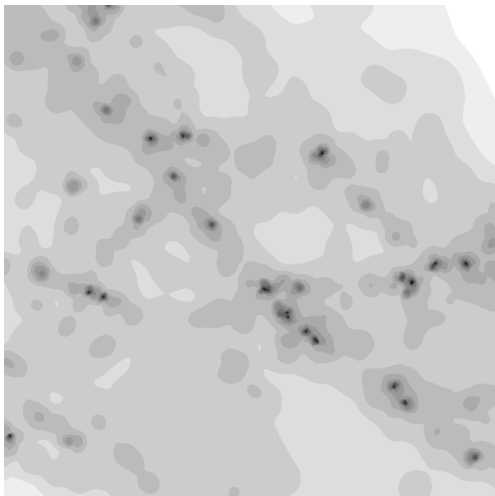


FIGURE 6. Right: HI column density map of a galaxy forming environment at at redshift $z=3$. Light gray correspond to column densities of about $\log N = 13.5$, dark gray to $\log N \approx 15.5$ and black to $\log N > 17.5$. Left: the same simulation shown as an artificial I-band image in an HDF-like exposure. Each frame has a side length of 2.8 Mpc (comoving).

ticular, they find that if they embed their disk model within a CDM structure formation scenario, the result is inconsistent with the observed velocity widths. However, although Prochaska & Wolfe investigated quite a number of different geometrical and dynamical configurations, all models have in common that the underlying mass distribution is highly symmetric and the models are in dynamical equilibrium.

The importance of asymmetries and non-equilibrium effects has been demonstrated by Haehnelt, Steinmetz & Rauch (1998). Figure 7 shows a typical configuration which gives rise to a high redshift DLAS with an asymmetric SiII absorption profile. The velocity width of about 120 km/s is also quite similar to typical observation. However, no large disk has yet been developed and also the circular velocity of the collapsed object is only 70 km/s. The physical structure which underlies DLASs are turbulent gas flows and inhomogeneous density structures related to the merging of two or more clumps, rather than large rotating disks similar to the Milky Way. Rotational motions of the gas play only a minor role for these absorption profiles. A more detailed analysis also demonstrates that the numerical models easily pass the statistical tests proposed by Prochaska and Wolfe, i.e., hierarchical clustering, in particular the CDM model, is consistent with the kinematics of high- z DLASs. Semianalytical models failed since they are based on the assumption of relaxed disk-like structures rather than the complicated infall pattern seen in the simulations.

7. Summary and Conclusion

Numerical simulations of the formation of galaxies through hierarchical clustering have been presented. The simulation outcome has been compared to a large variety of observations for galaxies at low and high redshifts. The main conclusions are the following:

- Hierarchical clustering has proven to be a very successful model for structure formation in the universe. It also provides well defined initial conditions from which the

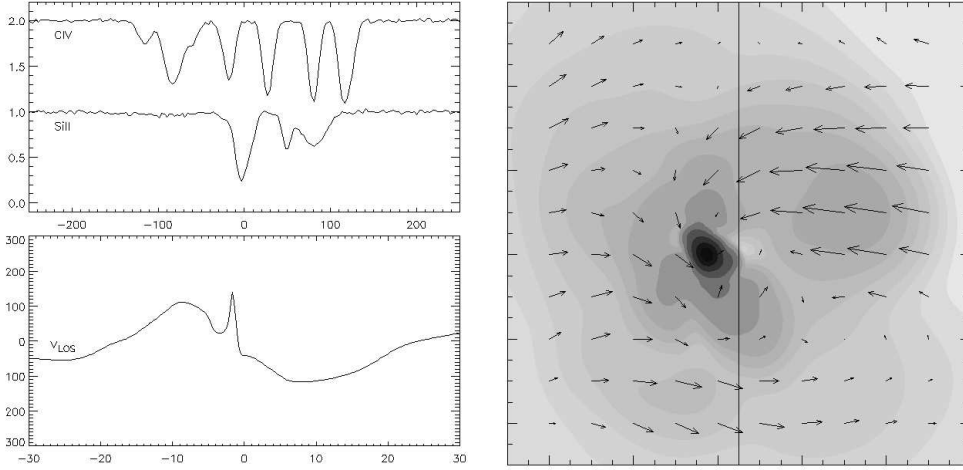


FIGURE 7. Right: Color map of the column density distribution in a 60 kpc around a damped system. Black correspond to HI densities $\log n(\text{HI}) > 1.5$, light grey to $\log n(\text{HI}) \approx -3$. White arrows indicate the velocity field. The white line correspond to the line-of-sight(LOS). In the lower left plot, the velocity field along the LOS is shown. The upper left plot shows the absorption line in CIV 1548 (top) and SiII 1808 (bottom). For readability, CIV has been displaced by 0.5 in flux.

formation of galaxies can be studied. Some observations like, e.g., the increasing evidence for redshift clustering are natural predictions of the hierarchical clustering hypothesis.

- Numerical simulations are an extremely powerful tool to study the formation of galaxies. Only numerical simulation can take full account of the dynamic of the formation process and the complicated interplay between different physical processes such as, e.g., accretion and merging, star formation and feedback, photo heating and radiative cooling.
- Overall, the qualitative picture seems to be fairly consistent, although current models still fail to reproduce the properties of the observed galaxy population in a quantitative manner. Future investigation will have to cope with the effects of (large-scale) star formation and feedback processes.

This article includes work from collaborations with G. Contardo, M. Haehnelt, J. Navarro and M. Rauch.

Appendix A. Simulating Galaxy Formation

A.1. Numerical method

The simulation presented in this article have been performed using GrapeSPH (Steinmetz 1996), a particle method that combines the hardware N -body integrator GRAPE (=GRAvity PipE, Sugimoto et al., 1990) with the Smooth Particle Hydrodynamics (SPH) approach to numerical hydrodynamics (Lucy 1977; Gingold & Monaghan 1977). GrapeSPH is fully Lagrangian, free from symmetry restrictions, and highly adaptive in space and time through the use of individual particle timesteps and smoothing lengths. The physical processes implemented in this code include self-gravity, gas pressure, hydro-

dynamical shocks, radiative cooling and heating by a photoionizing background, and star formation.

A.2. *Star formation*

Star formation is modeled by the creation of collisionless “star” particles in regions where the gas is locally Jeans unstable and where the cooling timescale is shorter than the local dynamical timescale. The local star formation rate per unit volume is assumed to be directly proportional to the gas density and inversely proportional to a local dynamical timescale. A star formation efficiency of 3% has been used (for details see Katz 1992; Navarro & White 1993; Steinmetz & Müller 1994, 1995), a value consistent with that observed in the Milky Way.

The orbits of newly formed stars are subsequently followed in a self-consistent fashion, assuming that they are only affected by gravitational forces. Young star particles devolve energy and metal enriched mass to their surrounding gas, an effect that mimics the energy and mass input by supernovae and evolving stars into the ISM. The supernova energy is added to the thermal energy of the surrounding gas. Input in kinetic energy (Navarro & White 1993) has not been assumed, i.e., this star formation model represents a minimum feedback model.

A.3. *Initial conditions and simulation design*

The large dynamic range needed to resolve the internal structure of galaxies and the full cosmological context of the galaxy formation process is achieved using a two-step procedure. First, galaxy-sized halos are extracted from large cosmological N-body simulations. Second, these systems are resimulated in high-resolution individual runs that use the same initial conditions and tidal fields of the original simulations plus small scale perturbations introduced to account for the increased Nyquist frequency of the second run (Navarro, Frenk & White 1995).

REFERENCES

- Barnes, J. 1988, ApJ, 331, 699.
 Baugh, C., Cole, S., Frenk, C.S., Lacey, C., 1998, ApJ, submitted (astro-ph/9703111)
 Cen, R., Miralda-Escudé, J., Ostriker, J.P., Rauch, M., 1994, ApJ, 437, L9
 Contardo, G., Steinmetz, M., Fritze-von Alvensleben, U., 1998, in preparation.
 Cole, S.M., Aragón-Salamanca, A., Frenk, C.S., Navarro, J.F., Zepf, S.E. 1994, MNRAS, 271, 781.
 Dekel, A., & Silk, J. 1986, ApJ, 303, 39.
 Efstathiou, G.P. 1992, MNRAS, 456, 43p.
 Elston, R., Bechtold, J., 1998 in preparation.
 Fall, S.M. 1983, in *Internal Kinematics and Dynamics of Galaxies*, Athanassoula E. (ed.), (Dordrecht: Reidel), p. 391.
 Fall, S.M. & Efstathiou, G. 1980, MNRAS, 193, 189.
 Frenk, C.S., White, S.D.M., Efstathiou, G.P., and Davis, M. 1985, Nature, 317, 595.
 Gingold, R.A., Monaghan, J.J., 1977 MNRAS, 481, 375.
 Haehnelt, M., Steinmetz, M., Rauch, M., 1996, ApJ, 465, L95.
 Haehnelt, M., Steinmetz, M., Rauch, M., 1998, ApJ, in press (astro-ph/9706201).
 Katz, N., 1992, ApJ, 391, 502.
 Katz, N., Weinberg, D. H., Hernquist, L., & Miralda-Escudé J. 1996, ApJ, 457, L57
 Kauffmann, G., Nusser, A., Steinmetz, M., 1997, MNRAS, 286, 795.

- Kauffmann, G., White, S.D.M., & Guiderdoni, B. 1994, MNRAS, 267, 981.
- Lucy, L., 1977, AJ, 82, 1013.
- Navarro, J.F., Frenk, C.S., & White, S.D.M. 1995, MNRAS, 275, 56.
- Navarro, J.F., Steinmetz, M., 1997, ApJ, 471, 13.
- Navarro, J.F., White, S.D.M., 1993, MNRAS, 265, 271.
- Pascarelle, S.M., Windhorst, R.A., Keel, W.C., Odewahn, S.C., Nature, 383, 45.
- Pierce, M.J., Tully, R.B., 1992, ApJ, 387, 47.
- Prochaska, J. X., & Wolfe, A. M. 1998, ApJ, in press, (astro-ph/9704169)
- Quinn, P.J. & Zurek, W.H. 1988, ApJ, 331, 1.
- Quinn, T., Katz, N. & Efstathiou, G. 1996, MNRAS, 278, L49.
- Rauch, M., Haehnelt, M.G., Steinmetz, M., 1997, ApJ481, 601.
- Silk, J., 1997, ApJ, 481, 703.
- Songaila, A.; Cowie, L. L., Hogan, C. J., Rugers, M., 1994, Nature, 368, 599.
- Steidel, C., Giavalisco M., Pettini, M., Dickinson, M., Adelberger, K., 1995, ApJ, 462, L17
- Steidel, C., Adelberger, K., Dickinson, M., Giavalisco M., Pettini, M., Kellogg, M., 1997, ApJ, in press.
- Steinmetz, M., 1996, MNRAS, 278, 1005.
- Steinmetz, M., 1997, *Numerical Simulations of Galaxy Formation*, Proc. *Science with the VLT*, Garching, Germany, April 1 - 4 1996, Springer Verlag Berlin Heidelberg, 156.
- Steinmetz, M., Müller, E., 1994, A&A, 281, L97.
- Steinmetz, M., Müller, E., 1995, MNRAS, 276, 549.
- Sugimoto, D., Chikada, Y., Makino, J., Ito, T., Ebisuzaki, T. & Umemura, M. 1990, Nature, 345, 33.
- Tytler, D., Fan, X.-M., Burles, S., 1996, Nature, 381, 207.
- Vogt, N., et al., 1997, ApJ, 479, L121.
- Weinberg, D., Hernquist, L. & Katz, N. 1997, ApJ, 477, 8.
- Windhorst, R., et al., 1994, ApJ, 435, 577.
- White, S.D.M., 1994, Les Houches Lectures
- White, S.D.M., Rees, M.J. 1978, MNRAS, 183, 341.
- White, S.D.M., Navarro, J.F., Evrard, A.E., Frenk, C.S., 1993, Nature, 366, 429.
- Wolfe, A. M. 1988, in *QSO Absorption Lines: Probing the Universe*, Proc. of the QSO Absorption Line Meeting, Baltimore, 1987, Cambridge University Press
- Zhang Y., Anninos P., Norman M.L., 1995, ApJ, 453, L57